Ion-Responsive Channels of Zwitterion-Carbon Nanotube Membrane for Rapid Water Permeation and Ultrahigh Mono-/Multivalent Ion Selectivity

Tian-Yin Liu,[†] Hao-Ge Yuan,[†] Qian Li,[†] Yuan-Hui Tang,[†] Qiang Zhang,[‡] Weizhong Qian,[‡] Bart Van der Bruggen,[§] and Xiaolin Wang*[,†]

[†]Beijing Key Laboratory of Membrane Materials and Engineering, Department of Chemical Engineering, Tsinghua University, Beijing 100084, PR China, [‡]Beijing Key Laboratory of Green Chemical Reaction Engineering and Technology, Department of Chemical Engineering, Tsinghua University, Beijing 100084, PR China, and [§]Department of Chemical Engineering, Process Engineering for Sustainable Systems, KU Leuven, 3000 Leuven, Belgium

ABSTRACT The rational combination of polymer matrix and nanostructured building blocks leads to the formation of composite membranes with unexpected capability of selectivity of monovalent electrolytes and water, which affords the feasibility to effeciently remove harmful ions and neutral molecules from the environment of concentrated salines. However, the multivalent ion rejection in salined water of routine nanocomposite membranes was less than 98% when ion strength is high, resulting in a poor ion selectivity far below the acceptable value. In this contribution, the ion-responsive membrane with zwitterion-carbon nanotube (ZCNT) entrances at the surface and nanochannels inside membrane has been proposed to obtain ultrahigh multivalent ion rejection. The mean effective pore diameter of ZCNT membrane was dedicated tuned from 1.24 to 0.54 nm with the rise in Na_2SO_4 concentration from 0 to 70 mol m^{-3} as contrary to the conventional rejection drop in carbon nanotube (CNT) membrane. The ultrahigh selective permeabilities of monovalent anions against divalent anions of 93 and against glucose of 5.5 were obtained on ZCNT membrane, while such selectivities were only 20 and 1.6 for the pristine CNT membrane, respectively. The ZCNT membranes have potential applications in treatment of salined water with general NaCl concentration from 100 to 600 mol m^{-3}, which are widely applicable in desalination, food, and biological separation processes.

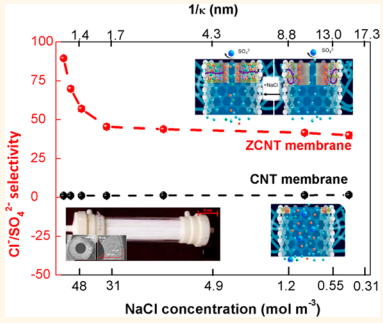

KEYWORDS: membrane · carbon nanotubes · ion-responsive · zwitterion

Water purification systems with superior performance for brackish water desalination and removal of harmful ions from contaminated water are strongly considered to address safe drinking water issues at a low cost.[1] The removal of harmful ions and neutral molecules from the environment of concentrated salines showed extremely high energy cost with low efficiency in desalination of brackish water, wastewater treatment of petrochemical, chlor alkali and texile industries.[2] The use of membrane for nanofiltration and reverse osmosis, which is currently the most energy efficient large-scale desalination process, leads to size-selectivity process that allows water to permeate but hinders the passage of ions.[3] However, due to enlargement of pore size as well as hindrance of electrostatic repulsion, the rejections of multivalent ions and small molecules become very low and thus poor selectivity when the saline concentration is elevated (*e.g.*, larger than 100 mol m^{-3} in wastewater and up to 600 mol m^{-3} in seawater).[4−7] Instead, it is necessary to control the nanostructure and the chemical functionality to obtain membranes that permeate ions preferentially. Up to now, lyotropic liquid crystals,[8] charge mosaic nanotubes,[9] and aquaporins[10] render the purification process with the ability to remove various contaminants from water in a single step with a high solute selectivity and large water permeability.[11,12] If an ion-responsive building block can be rationally integrated into a membrane, the rejection as well as the separation of ions are expected to be well tuned to efficiently harvest clean water.[13−15] It is also highly required to effectively separate

* Address correspondence to xl-wang@tsinghua.edu.cn.

Received for review April 30, 2015 and accepted July 8, 2015.

Published online July 08, 2015
10.1021/acsnano.5b02598

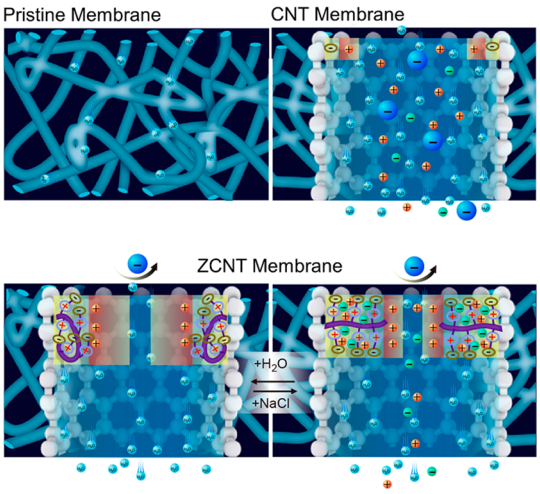

Figure 1. Schematic diagram of ion-responsive poly-(zwitterions) on CNT membrane with rapid water channels and ultrahigh mono/multivalent ion selectivity. (a) Water molecules and monovalent ions permeated through the tortuous water channels of pristine membrane. (b) The CNT membranes afforded large water channels, which were lack of ion selectivity. (c) The PSB layer in the "super-collpased state" were grafted on the CNT tips, which were in the "nanoconfined stretching state"induced by the ionic responsive performance (shown in d) and served as water channels and high mono/multivalent ion selectivity.

mono/multivalent anions and neutral molecules/monovalent electrolytes that are widely employed in desalination, food, and biological separation processes.[1,16]

The emergence of nanocarbons offers ubiquitous water channels based on carbon nanotubes (CNTs) and proton pathways based on graphene.[17−23] The CNT composite membranes with nanoscale channels exhibit rapid water permeation, cost effectiveness, and processing scalability.[16,24−26] Therefore, CNT composite membranes are a promising alternative to ultralow porous and high tortuous nanofiltration membranes (Figure 1 (a)).[5,17] However, the pristine CNT composite membranes have been found to exhibit poor abilities to remove small molecules and electrolyte from water, as well as no selectivity for mono/multivalent anions (Figure 1 (b)).[27] Both positively charged (*e.g.*, amine groups) and negatively charged (*e.g.*, carboxyl groups) tip functionalizations have been explored for improving electrostatic repulsion to reduce permeation of multivalent ions, while the ionic permeability is improved dependent on the ionic strength, dominated by the "screening effect" of the thinner electric double layer with enlarged cross section of nanotubes.[28] In contrast, the ionic permeability is usually rapid without selectivity at a high ionic strength.[29] Furthermore, the rigid rods of the functional groups blocked the water channels, which is unfavorable for rapid permeation of water.[30] Recently, the superhydrophilic chemistry of tips of CNTs was found to reduce the entrance energy for water molecules because of the strong ion-dipole interaction.[15] The nanoconfinement of water molecules inside nanopores hinders the permeance of ions and neutral molecules through the exclusive effect induced by the nanopore structure and chemistry.[31] Rational design of tip functionalized CNT membrane with superhydrophilicity is highly desirable for efficient separation purpose, which is attributed by dielectric exclusion triggered by nanoconfinement.[32,33]

In this contribution, an ion-responsive CNT membrane was developed with rapid water channels and ultrahigh mono/multivalent ion selectivity. Poly(sulfobetaine) (PSB) brushes were employed as the gatekeepers at the tip of CNTs in the poly(zwitterionic) CNT (ZCNT) membrane. The reason why PSB was selected related to the ion-responsiveness of PSB chains. The configuration of PSB can be easily modulated by the ionic strength of mono/multivalent electrolytes.[34] PSB chains can be grafted from CNTs and contributed nanoporous gates with controllable pore size, and the mechanism of stimuli-responsive performances of selectivity was presented as Figure 1. With the rise in the ionic strength of electrolytes, the PSB chains were tuned from "super-collapsed state" into the nanoconfined state (Figure 1 (c, d)). Consequently, the pores along the *c*-axis of CNTs became narrow when CNTs served as rapid water channels (Figure 1 (d)). Based on these considerations, PSB chains were grafted on CNTs in the membrane. The as-obtained ZCNT membranes delievered an ionic responsiveness in terms of pore narrowing with increasing ion concentration. The selectivities of monovalent ions against both the neutral molecules and multivalent ions were explored for mono/multivalent ion separation process. The ion-responsive ZCNT membranes yielded 1-fold higher permeabilities and more than 5−10 times larger fluxes in modules than that of pristine membrane can accommodate.

RESULTS AND DISCUSSION

The Structures of Nanoporous ZCNT Membranes. PSBs are extraordinary building blocks for molecular separations with supermolecular assembly and superhydrophilicity.[35] A typical microstructure of the ZCNTs grafted by PSB was fabricated by a Ce-initiating atom transfer radical polymerization. The ZCNTs exhibited a coaxial cable structure, in which the cylindrical CNTs served as the core and the PSB layers employed as the skin (Figure 2a). The PSB layers were grafted from both the outer layers and tips of porous CNTs, resulting in a controllable thickness ranging from 1.13 to 3.68 nm. Due to the relative dense and thick PSB layers, the end-opened tips were filled with the macromolecular chains. With increasing the monomer/initiator molar ratio from 0.01, 0.02, 0.03, to 0.04, the PSB layer of ZCNTs gradually evolved from inside surface to the thicker PSB layer of ZCNT-1 (1.13 nm PSB), ZCNT-2 (1.08 nm PSB), ZCNT-3 (2.08 nm PSB), and ZCNT-4 (3.68 nm PSB) (Figure S1 and S2). The PSB soft chains were solidly supported by the nanopores when the

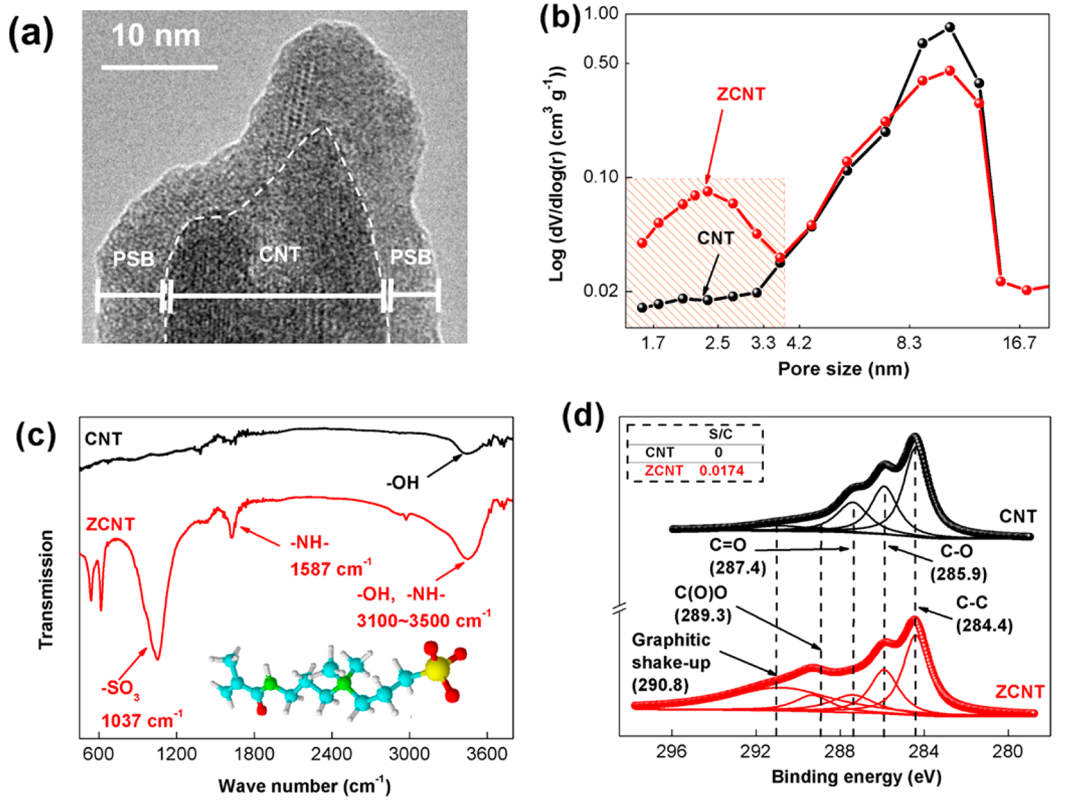

Figure 2. Characterizations of ZCNTs: (a) TEM image of CNTs with ion-responsive PSB layer, (b) the pore size distribution, (c) the ATR-FTIR profiles, and (d) the C 1s XPS plots of CNTs and ZCNTs.

thickness of PSB layer exceeded the nanopore radius, *e.g.*, 2−5 nm (Figure 2b). Otherwise, the PSB layer was found to collape and leakage under hydraulic pressures, especially in the case of soft networks.[36,37] For this reason, ZCNT-3 with PSB layer thickness of 2.1 nm was selected as the model ZCNT membrane to demonstrate the role of ion-responsive poly(zwitterions), while the pristine short CNTs with a length of *ca.* 100 nm were employed as the control sample in this contribution.

The detailed textures of ZCNTs were further probed by the N_2 sorption. The pore size distribution of ZCNTs were presented as Figure 2b and S1b. The CNTs delivered nanopores with a single peak distribution between 3 and 15 nm, while the ZCNTs exhibit a bimodal peak distribution at 1.7−3.0 and 3.5−15 nm, respectively (Figure 2b). There were abundant nanopores in the ZCNTs ranging from 1.7 to 3.0 nm by grafting PSB layers at the CNT tips. The nanopores were ascribed to the space between the macromocular coiled-chains. The mesoporosity of ZCNTs decreased to 0.43 from 0.90 $cm^3\ g^{-1}$ of CNTs. Larger uptakes for ZCNTs (0.09 $cm^3\ g^{-1}$) at low relative pressures (Figure 2b, shadow area) indicate more prominent nanoporosity. It was dramatically greater than that of CNTs (0.02 $cm^3\ g^{-1}$) due to the introduction of the assembled PSB layers. With more PSB chains onto CNTs, more nanopores can be found in the ZCNT samples (Figure S1b). The ZCNTs were dominated as loose coiling structures in "super-collapsed state" (Figure 1 (b)). Such "super-collapsed structure" was attributed from the intramolecular interactions between ionized zwitterionic brushes on the PSB side chains that bore both negative (sulfonate, $-SO_3^-$) and positive (amine, $-N^+(CH_3)_2-$) charge units. This was validated by the vibration peaks at 1050 cm^{-1} ($-SO_3^-$)) and 1560 cm^{-1} (−NH−) of attenuated total reflectance (ATR)-Fourier transform infrared (FTIR) profiles (Figure 2 and S3c). The stacking density was determined by the length ratio between the thickness of PSB layer in "super-collapsed state" and the relaxation state, which deviated from 1 with reduced interchain interaction. The mean chain length (ML, nm) in relaxed state was calculated by the assumpation that the flexible chains had topologies in a Gauss model with a rigid chain unit of 0.78 nm.[15] The polymerization degree was inferred by sulfonate/ether carbon (C(O)O) ratio that determined by the S/C ratio *via* X-ray photoelectron spectroscopy (XPS) analysis. The relative amount of C(O)O carbon (289.3 eV) was obtained by the deconvolution of C 1s spectrum shown in Figure 2d, among C−C (284.4 eV), C−O (285.9 eV), C═O (287.4 eV), and graphitic shakeup satellites (290.8 eV) components. The stacking density of ZCNT-1 (0.42), ZCNT-2 (0.28), ZCNT-3 (0.36), and ZCNT-4 (0.48) were far from 1.0, indicating the coiling of polymer chains. The result indicated that the flexible chains were in "super-collapsed state" for all ZCNT samples (Figure S3).

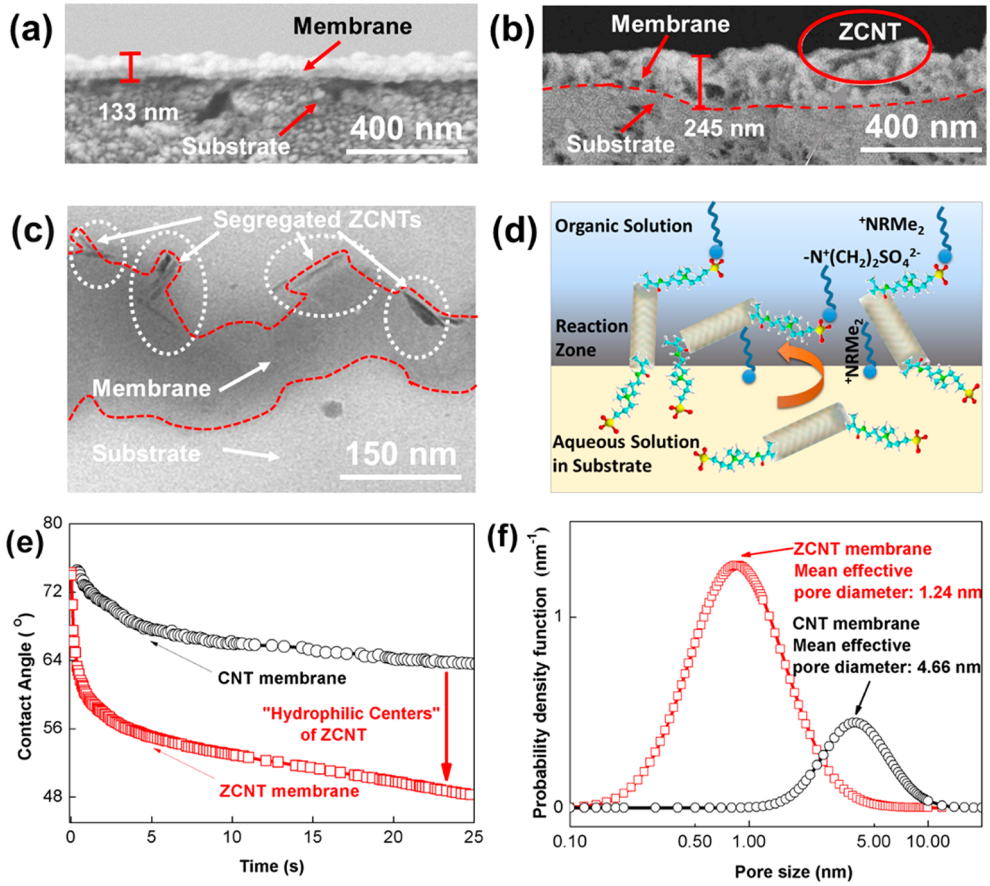

Figure 3. Morphologies and properties of the ZCNT and CNT membranes: SEM image of cross-sectional structure of (a) pristine and (b) ZCNT membrane; (c) TEM image of cross-sectional structure of ZCNT membrane; (d) schematic illustration of the fabrication process for ZCNT membrane; (e) the dynamic contact angle curves and (d) the pore size distribution profiles of ZCNT and CNT membranes.

The ZCNTs were assembled into an ultrathin membrane with a thickness of around 100 nm (Figure 3a). The interfacial compatibility between ZCNTs and the polyamide substrate was ensured by the hydrogen bondings between the amide groups within the polyamide frameworks and the ester groups on ZCNTs (Figure 3b). Because the dense structure in the ultrathin membrane near surface dominates the permeance and separation performances, the ZCNTs were transferred to the outside surface through interfacial segregation, achieved by pulling the sulfonic acid groups of zwitterionic tips on ZCNT ends toward the alkyl ammonium salt in the reaction zone of orgainc phase *via* the "salt bridge" (Figure 3d). The ZCNT tips were extruded from the outer surface of the composite membrane (Figure 3c). The interfacial activating agent of hexadecyltrimethylammonium bromide prevented the agglomeration and immersion of ZCNTs in the polymeric networks, which improved the nanoporosity on the membrane surface for direct water permeation (Figure S4). It was further confirmed by the larger roughness (231 nm) compared to the pristine membrane (75 nm) determined by atomic force microscope (Figure S5). In order to verify the effect of straight ZCNTs on the water diffusion in the membrane, the membrane tortuosity (τ) was determined by the Spiegler–Kedem equation based on the structural parameter, $A_k/(\tau \times \Delta x)$ (Figure S6 and Figure S7). The minimum τ valune of 1.5 was obtained in the ZCNT-3 membrane with a ZCNT incorporation ratio of 0.1 wt %. This was three times lower than that of the pristine membrane (τ = 4.9). However, further incorporation of ZCNTs with a ratio of 0.2 wt % resulted in an undesirable enlargement of τ to 2.5, arising from clogging between the intertube defects (Figure S7). The improved pure water flux from ZCNT membrane (0.025 wt %) of 0.21 mol m^{-2} s^{-1} to ZCNT membrane (0.1 wt %) of 0.29 mol m^{-2} s^{-1} and subsequently loss in pure water flux of ZCNT membrane (0.2 wt %) to 0.23 mol m^{-2} s^{-1} provided direct evidence for the τ change (Figure S5). Compared to the CNT membrane, the ZCNT membrane herein provided not only the ion-responsive "gate" structure by tip functionalization that preserved the separation, but also the rapid water channels with the segregated ZCNTs that were directly contacting with water molecules on membrane surface. Consequently, it ensured the short pathways in the bulk as verified by the ultralow τ of ZCNT membranes (Figure 3d).

The ZCNTs segregating on the membrane surface ensured good contact between the feed solution and

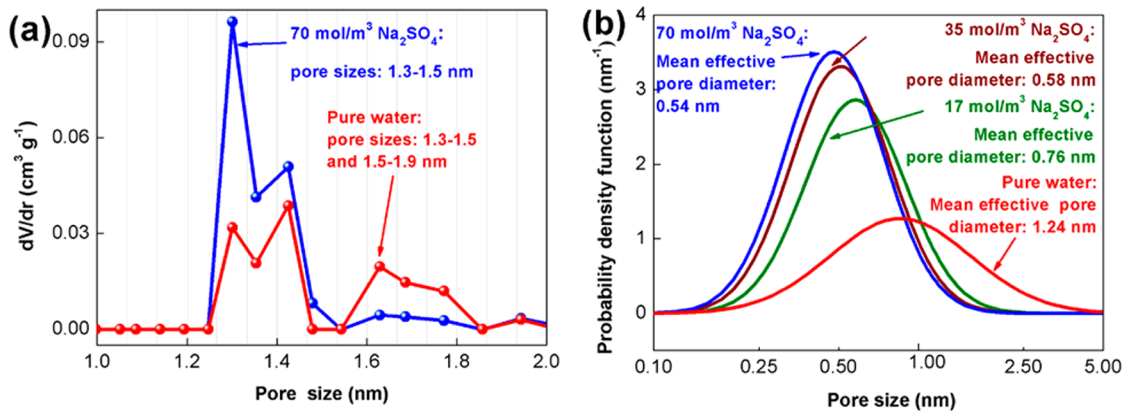

Figure 4. Ion-responsive performance of ZCNT membranes: (a) the pore size distributions of the ZCNT membranes before and after filtration of 70 mol m^{-3} Na_2SO_4 calculated by DFT method from the nitrogen sorption isotherm; (b) the mean effective pore diameter of ZCNT membrane obtained by log-normal fitting method in dextran solutions.

nanoporous ZCNT tips, which was beneficial for the preferential adsorption of water. The dynamic contact angle profiles of the ZCNT membrane exhibited a considerably steeper slope at the initial stage than the pristine CNT membrane, which indicated that the "hydrophilic centers" on the ZCNT membrane surface delivered an ultralow hydration energy for water molecules. Therefore, the ZCNT membrane yielded a much quicker entrance of water molecules into the channels (Figure 3e). By forming the nanoporous "gates" on the membrane surface, the ZCNT membrane rendered a much narrower mean effective pore diameter (1.24 nm) than that of CNT membrane (4.66 nm) (Figure 3f), which were introduced in Table S1 and S2.

The Filtration Performance of ZCNT Membranes. The ion responsive gate was probed by the pore size distributions of dry and wet ZCNT films after filtration of 70 mol m^{-3} Na_2SO_4 solution. The mean effective pore diameters of the ZCNT membranes in dry state were characterized by N_2 adsorption and analyzed by density functional theory (DFT) as shown in Figure S8. The nanopores of ZCNTs were mainly in the range of 1.0−1.9 nm (Figure 4a). After filtrating of the Na_2SO_4 solution, the reorganization of poly(zwitterionic) brushes induced the translation of the super-collapsed state with nanocavities (1.5−1.9 nm) into the nanoconfined stretching state with narrower nanopores (1.0−1.5 nm) (Figure 4a). The nanoconfined brushes tended to stretch in water. The increasing ionic strength (Na_2SO_4 from 0, 17, to 35 mol m^{-3}) induced a shift from intrinsic to extrinsic charge compensation. The mean effective pore diameter decreased dramatically from 1.24, 0.76, to 0.58 nm. This was consistent with the entropic gain of the poly(zwitterions) to the nanoconfined stretching until the ionic strength reached a point (70 mol m^{-3}) where counterion release has hardly any entropic gain, corresponding to a mean effective pore diameter of around 0.57 nm (Figure 4b).

In order to demonstrate the potential of ZCNT membranes for molecular separations, the water permeation and ionic separation performance were further investigated on aqueous Na_2SO_4 solutions with different concentrations. The water permeability (L_p) of ZCNT membrane (0.29 mol m^{-2} s^{-1}) is significantly larger than that of the pristine membrane (0.17 mol m^{-2} s^{-1}) (Figure S6). Compared to the larger incorporation ratio (*e.g.*, 20 wt %) to achieve the same order of enhancement in water permeability, the permeation of ZCNT membrane is significantly improved at extremely incorporation ratio (*e.g.*, 0.1 wt %), dominated by the rapid permeation of ZCNTs.[30] The L_p in Na_2SO_4 solution of the ZCNTs and pristine membrane changes in different ways: compared with a nearly horizontal L_p curve (slightly increases from 0.29 to 0.30 mol m^{-2} s^{-1} bar^{-1}) of pristine membrane, the L_p of ZCNT membrane slightly decreased from 0.29 to 0.25 mol m^{-2} s^{-1} bar^{-1} by rising Na_2SO_4 concentration (Figure 5a). Such moderately dropped profile of L_p reflected the growing transport resistance, as supported by the narrower pore sizes in Figure 4b. Thus, the ZCNT membrane exhibited 1 order of magnitude rapid water permeation than previous reported CNT membranes using single-walled CNTs (0.021 mol m^{-2} s^{-1} bar^{-1})[30] because of the naonporosity of supramolecular architecture at CNT tips, as well as multiwalled CNTs (0.042 mol m^{-2} s^{-1} bar^{-1})[27] attributed from the surface exposure of ZCNT channels.

The dependence of the SO_4^{2-} permeability on the electrolyte concentration was further investigated (Figure 5b). The CNT channels were negatively charged due to the carboxyl acid groups at tips, characterized by the zeta potential of −9.0 mV. The electrostatic repulsion between the carboxyl and SO_4^{2-} groups became weaker when the surface charges were gradually shielded by the higher Na^+ concentration in solution. This was proved by the gradually reduced electric interaction distance that was represented by narrower Debye length ($1/\kappa$, 9.8−1.8 nm) with the rise of Na_2SO_4 concentration from 0.7 to 70 mol m^{-3}. Therefore, the CNT membrane exhibited an extremely low SO_4^{2-} permeability of 2.1×10^{-7} at 0.7 mol m^{-3} Na_2SO_4 concentration, while suffered from severe leakage

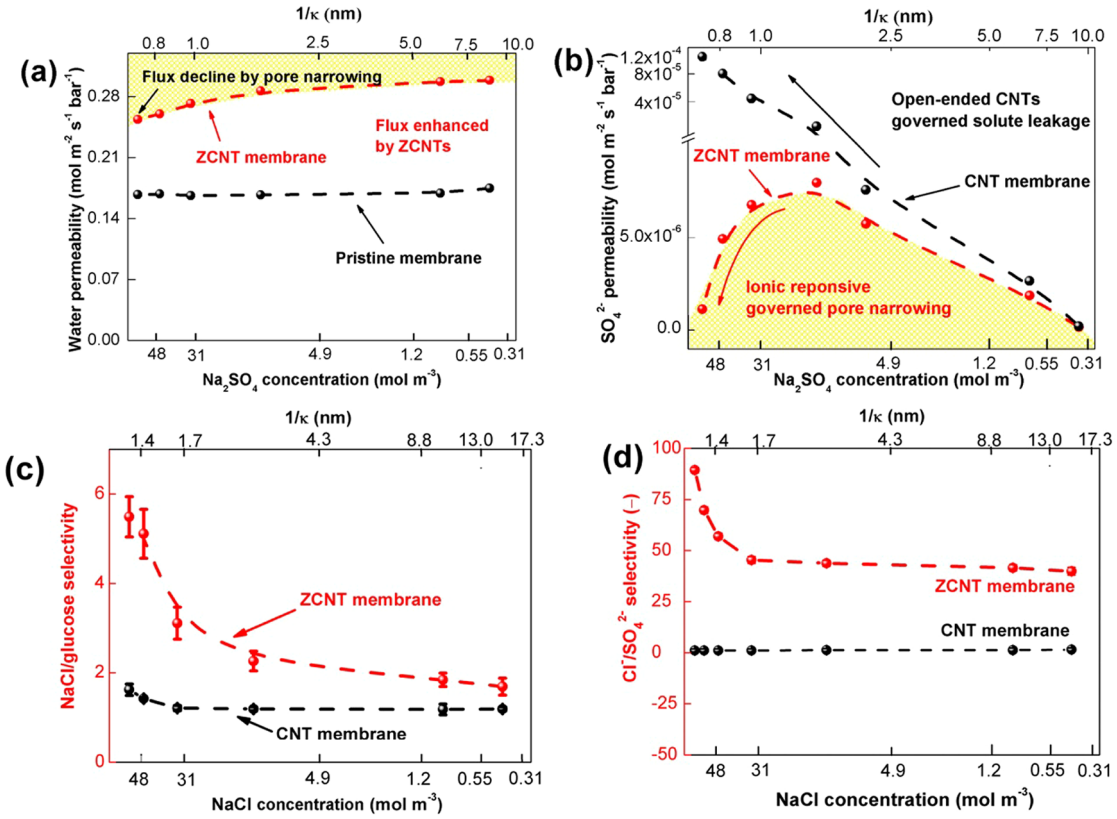

Figure 5. Application of ZCNT membrane with ion-responsive poly(zwitterions): (a) the water permeability of ZCNT and pristine membranes; (b) the SO_4^{2-} permeability of ZCNT and pristine membrane in Na_2SO_4 solutions from 0.7 to 70 mol m^{-3}, corresponding to SO_4^{2-} Debye length ($1/\kappa$) from 9.7 to 0.7 nm; (c) the selectivity of NaCl/glucose and (d) the selectivity of Cl^-/SO_4^{2-} ion in mixtures with NaCl concentrations from 0.7 to 70 mol m^{-3}.

of 3 orders of magnitude larger permeability (1.2×10^{-4} mol m^{-2} s^{-1} bar^{-1}) with a rise of Na_2SO_4 concentration to 70 mol m^{-3}. The ZCNT membrane with a mean effective pore diameter of 1.2 nm yielded three-magnitude-lower SO_4^{2-} permeability than CNT membrane (mean effective pore diameter of 4.4 nm) at all tested ionic strengths. Interestingly, a "volcano curve" was found in the SO_4^{2-} permeability−ionic strength profile (Figure 5b). The ion permeability was retarded by the poly(zwitterions) at tips and reduced the transmittion into nanotubes from the bulk solution. Because the zwitterions were uncharged near the isoelectric point of pH = 7, the ZCNT charge was sufficiently low (corresponding to a zeta potential of −2.5 mV) to develop weak electric repulsion at the surface. The ZCNT membrane delivered slightly increased SO_4^{2-} permeability from 1.5×10^{-7} to 7.8×10^{-6} mol m^{-2} s^{-1} bar^{-1} at extremely low Na_2SO_4 concentrations (0.3−17.0 mol m^{-3}), corresponding to SO_4^{2-} rejections dropped from 98.5 to 97.6%. Interestingly, the SO_4^{2-} permeability reduced from 7.8×10^{-6} to 1.1×10^{-6} mol m^{-2} s^{-1} bar^{-1} by rising Na_2SO_4 concentration from 17 to 70 mol m^{-3}. Triggered by the nanoporous narrowing from 0.76 to 0.54 nm, SO_4^{2-} transmission was strongly influenced by dielectric repulsion due to the high valent state of SO_4^{2-} anions (Stokes diameter: 0.76 nm). Thus, the SO_4^{2-} ions were strongly repelled from the tips and revealed diffusion more slowly, while the smooth walls of ZCNTs allowed rapid diffusion of water molecules with sizes of 0.28 nm (Figure 4b).

Ultrahigh Selectivity of ZCNT Membranes with Nanoconfined Stretching Structure. According to the tunable nanopore size in an elevated ionic-responsive approach, the nanopores of the ZCNT membrane with a minimized diameter of 0.54 nm had strong steric repulsion with either monovalent cations (Na^+: 0.72 nm) or anions (Cl^-: 0.66 nm). The ultralow rejection of NaCl in ZCNT membrane (less than 1%) was dramatically different from that in typical dense membranes (30−99.8%).[38] Thus, an ion-selective channel was found to selectively penetrate monovalent ions, *via* the formation of ($-N^+(CH_3)_2 \cdot Cl^-$) and ($-SO_3^- \cdot Na^+$) adsorbed the equal molar of Na^+ and Cl^- into the tubes through strong electrostatic attractions.[34] It was beneficial for high monovalent ionic diffusivity and simultaneously shielding zwitterionic groups to investigate the chain stretching on the selectivity against neutral molecules as well as multivalent ions. These nanopores rendered strong steric repulsion against neutral molecules, *e.g.*, glucose with a diameter of 0.77 nm. Consequently, the selectivity of NaCl/glucose through the ZCNT membrane increased to 5.5 with the rise of NaCl concentration (Figure 5c). It was significantly higher than that of the pristine membrane (around 1.6), which

was ascribed to the significantly rapid permeation of monovalent ions. Figure 5d exhibited the ZCNT membrane with reduced SO_4^{2-} and climbed Cl^- permeability than that of pristine membrane. An ultrahigh mono/multivalent anion selectivity, *e.g.*, Cl^-/SO_4^{2-} of 93 was obtained for the ZCNT membrane, while the selectivity was only 20 for the pristine membrane. The prominently larger selectivity was little influenced by the steric repulsion due to the similar stokes diameters of SO_4^{2-} (0.76 nm) and glucose (0.77 nm). Besides the steric hindrance, the dielectric exclusion took dominate effects in nanopores, especially in the range of 0.5−1.5 nm.[39] The solvation energy barrier of ions sharply increased when entering the nanopores, due to the dielectric constant dramatically drop in the nanotubes named as the "dielectric exclusion".[31] Thus, the Cl^-/SO_4^{2-} selectivity surpassed further than that of the Cl^-/glucose in the NaCl environment with a higher ionic strength. Such effect was specifically evident in this system, probably due to the water molecules surrendered severer nanoconfinement in a strongly ionized pore of poly(zwitterions). To further prove the effect, the ZCNT membrane showed the ionic selectivities of mono/multivalent anions (Cl^-/CO_3^{2-} and Cl^-/PO_4^{3-}) as well as mono/multivalent cations (Na^+/Mg^{2+} and Na^+/Al^{3+}) (Figure S9).

The poly(zwitterions) was an efficient and effective candidate to build ion-responsive membranes with improved selectivity of monovalent anions against neutral molecules and multivalent anions. A high nanocavity/free volume ratio with improved water permeability of 0.11 mol m^{-2} s^{-1} bar^{-1} was observed as a result of the increasing interchains of PSB but reducing intrachain electostatic interaction.[40,41] However, the strong molecular association of PSB nanoparticles induced large nanocavity size of 4.66 nm, and thus high divalent cation/anion leakages of 1.2−2.0 × 10^{-4} mol m^{-2} s^{-1} bar^{-1} and inferior selectivity of monovalent ion against divalent ions of 1.9.[41] Herein, the cylinder structure of CNTs shielded the molecular association and induced a stretching structure of the poly(zwitterions) brushes in the electrolyte solutions, which was called "anti-polyelectrolyte effect".[35] The assembly of PSB brushes in nanoconfined stretching state effectively formed nanoporous gates with ion-selective channels, which resulted in the reinforced monovalent permeability (*e.g.*, NaCl: 0.0034 mol m^{-2} s^{-1} bar^{-1}) while retarding permeability of the multivalent anions (*e.g.*, SO_4^{2-}: 7.7 × 10^{-6} mol m^{-2} s^{-1} bar^{-1}). By using the "anti-polyelectrolyte effect" of PSB through increasing the ionic strength of mono/multivalent electrolytes, the pore narrowing was expected by the transition from "super-collapsed state" into the nanoconfined state.[34] A sharp decrease of mean effective pore diameter of ZCNT membrane from 1.24 to 0.54 nm was observed with the rise of Na_2SO_4 concentration from 0 to 70 mol m^{-3}. Consequently, the selectivity of Cl^-/SO_4^{2-} was triggered by reorganizing the nanoporosity *via* retarded diffusion of the SO_4^{2-}. This effect was prominent because the dielectric exclusion of SO_4^{2-} was much larger than Cl^-, as a result of the extra secondary ionization energy of SO_4^{2-}. The inhibited NaCl permeability of 0.0012 mol m^{-2} s^{-1} bar^{-1} was observed with a relatively low water permeability of 0.06 mol m^{-2} s^{-1} bar^{-1}.[30] Compared to the commercial NF-90 membrane, the ZCNT membrane exhibited 2-fold larger water permeability (ZCNT: 0.29 mol m^{-2} s^{-1} bar^{-1} than NF-90:0.093 mol m^{-2} s^{-1} bar^{-1}), comparable Na_2SO_4 rejection (ZCNT: 99.9% than NF-90:99.75%) while much lower NaCl rejection (ZCNT: 1−8% than NF-90:50−60%).

Moreover, the fabricated ZCNT membrane could be assembled in a hollow fiber configuration (Figure S10). When assembled into a 2-in. module, ZCNT membranes afforded 10-fold higher module production (1.0 m^3 h^{-1}) than the routine modules using flat sheet membrane (*e.g.*, commercial NF-90 membrane). If the PSB chains were rationally grafted inner walls of CNTs, the sieving pores were further modulated as monovalent ion channels with rapid water diffusion but high mono/multivalent selectivity.

CONCLUSIONS

An ion-responsive ZCNT membrane with capability of selectivity of monovalent electrolytes and water in the presence of multivalent anions and neutral molecules was proposed and realized with poly(zwitterionic) PSB gatekeepers on pristine CNTs. The ion-responsive membrane was constituted ZCNTs entrances at the surface and penetrated through the bulk membrane. The mean effective pore diameter of ZCNT membrane was dedicated tuned from 1.24 to 0.54 nm with the rise in Na_2SO_4 concentration from 0 to 70 mol m^{-3}. Contrary to the conventional rejection drop in increasing electrolyte concentrations, the ZCNT membranes generally exhibited increasing separation capacities with Na_2SO_4 concentration raised from 0.7 to 70 mol m^{-3}. The ultrahigh selective permeabilities of monovalent anions against divalent anions of 93 and against glucose of 5.5 were obtained on ZCNT membrane, while such selectivities were only 20 and 1.6 for the pristine membrane, respectively. The ZCNT membranes have promising applications in desalination, food, and biological separation processes.

EXPERIMENTAL SECTION

Materials. CNTs with a length of *ca.* 10 μm and a diameter of about 15 nm were mass produced in a fluidized bed reactor.[42−44] The CNTs were first short-cut with a length of *ca.* 100 nm by an ultrasonic assisted chemical oxidization at 70 °C using a mixture of nitric acid (69 wt %) and sulfuric acid (98 wt %)

with a weight ratio of 3.0. After thorough washing, the short-cut CNTs (0.05 g) were oven-dried for further modification.

Fabrication of ZCNT Membranes. The short-cut CNTs were coated with PSB layers using the cerium (Ce (IV))-induced graft polymerization method. In brief, 1.0 g of short-cut CNTs were uniformly dispersed as 200 mL of degassed aqueous solution containing ceric ammonium nitrate (4.39 g), nitric acid (7.41 g), and 3-(methacryloylamino)propyl-dimethyl-(3-sulfopropyl) ammonium hydroxide (0.073 g) under nitrogen protection at 40 °C. The ZCNTs were obtained with conformal PSB layers after 1.5 h reaction. The ZCNTs were thoroughly washed with 50 mol m^{-3} phosphate-buffered saline (PBS, pH 7.4) solution for 3 times. Then the sample were further cleaned with deionized water for 1 h to full remove other impurities. The dark gray ZCNTs were obtained by the oven dry at 120 °C for 12.0 h.

The ZCNT membranes were fabricated by an interfacial polymerization (IP) process onto a hollow fiber substrate, which was similar to the pristine membrane fabrication.[45,46] Specifically, the dry hollow fiber substrate was wetted with the cross-linking solution of 0.06 wt % trimesoyl chloride (TMC) in dioxane/hexane (1:10) for 10.0 min. The IP process was then conducted for 2.0 min in the amine solution containing 2.0 wt % piperazine, 2.0 wt % piperazine/0.05−0.20 wt % CNTs, 2.0 wt % piperazine/0.05−0.20 wt % ZCNTs for the pristine, CNT, and ZCNT membrane, respectively. The post-treatment was carried out in 0.10 wt % TMC and 0.05 wt % hexadecyl trimethylammonium bromide/hexane solvent for 2 min, followed by 70.0 °C curing for 8.0 min. The pristine, CNT, and ZCNT membranes with nanocomposite barrier layers were prepared and stored in the buffer solution ($NaHSO_3$: 500 ppm at 4.0 °C) for further testing.

Characterization of Membrane Structure. The N_2 adsorption−desorption isotherms of the pristine, CNT, and ZCNT membranes were collected by an Autosorb-IQ2-MP-C adsorption analyzer. Before N_2 sorption isotherm measurements, every sample was degassed at a low temperature of 60 °C until a manifold pressure of 2.0 mmHg was achieved to avoid pore deformation. The mesoporosity was identified by the pore volume as determined by the Brunauer−Emmett−Teller (BET) method, and the pore size distribution plot of the dry membrane was calculated by the quenched solid DFT using the adsorption branch. The chemical bonding of the CNT/ZCNT membranes were characterized by Nicolet 6700 ATR−FTIR spectroscopy. The surface composition and bonding were detected by the ULVAC-PHI XPS. The microstructure and morphology of CNTs/ZCNTs and related membranes were observed using JEOL 7401F field emission scanning electron microscope (SEM) at an accelerating voltage of 3.0 kV and JEOL JEM2010 TEM at 80 kV. The SEM samples of CNT/ZCNT membranes were dried in a desiccator at a vacuum pressure of 0.9 bar and then were sputter coated with Pt at 10 mA for 5.0 min. The TEM samples of membrane were sliced into ultrathin sections with a thickness around 70 nm by a 701704 Reichert−Jung Ultramicrotome. The hydrophilicity of pristine, CNT, and ZCNT membranes were characterized by an OCA 20 dynamic contact angle meter at 25.0 °C. The surface roughness of pristine and CNT/ZCNT membrane was probed by a SPM 29500 AFM.

Evaluation of Filtration Performance. A cross-flow filtration system with four steel modules was employed for filtration measurements. The shearing velocity was kept at 60.0 L h^{-1}. The water fluxes (J_v, mol m^{-2} s^{-1}) were obtained by increasing the operational pressure (ΔP, bar) from 1 to 10 bar. The water permeability (L_p, mol m^{-2} s^{-1} bar^{-1}) was obtained by the slope of collected $J_v/\Delta P$ values. The observed transmission of the membrane ($Tr = C_p/C_f$) for a solute defines the ability of solute to pass through the membrane, where C_p and C_f (mol m^{-3}) are the solution concentrations of permeate and feed, respectively. The solute permeability is used to characterize the passing capability of the membrane against solute: $B = L_p \times (Tr)/(1 - Tr)$ (mol m^{-2} s^{-1}). The selectivity of two solutes through the membrane is represented by the ratio of their transmissions: $S_{(i/j)} = Tr_{(i)}/Tr_{(j)}$.The tested solutes included both electrolytes (Na_2SO_4, NaCl) and neutral molecules (ethyl alcohol, *n*-butyl alcohol, glucose, saccharose, raffinose, α-cyclodextrin, β-cyclodextran), characterized by using an ICP-OES inductively coupled plasma-optical emission spectroscopy and/or a TOC-VCPN total organic carbon analyzer.

The pore size distributions of the wetted membranes were obtained by fitting the rejections of neutral molecules ($R = 1 - C_p/C_f$) *via* a log-normal model, where C_p and C_f are concentrations in permeate and feed solution, respectively.[47] τ was obtained by electrostatic and steric-hindrance model:

$$\tau = \frac{A_k D_s (1 - r_s/r_p)^2}{\Delta x P_{neu}} \quad (1)$$

where A_k (−), P_{neu} (m s^{-1}), D_s (m^2 s^{-1}) and Δx (m) are surface porosity, permeability, diffusivity of neutral solute, and barrier layer thickness, respectively. The detailed information was shown in Figure S6.

Conflict of Interest: The authors declare no competing financial interest.

Acknowledgment. This work was supported by the National Key Technologies R&D Program of China (No. 2015BAE06B00), the National Natural Science Foundation of China (21422604, 21406128), and Tsinghua University Initiative Scientific Research Program (20121088039).

Supporting Information Available: The morphologies and C 1s XPS profiles of ZCNTs, AFM images and surface roughness of the ZCNT membrane, J_v − operational pressure profile and τ of the ZCNT membranes, ZCNT membrane in hollow fiber configuration and hollow fiber modules. The Supporting Information is available free of charge on the ACS Publications website at DOI: 10.1021/acsnano.5b02598.

REFERENCES AND NOTES

1. Shannon, M. A.; Bohn, P. W.; Elimelech, M.; Georgiadis, J. G.; Mariñas, B. J.; Mayes, A. M. Science and Technology for Water Purification in the Coming Decades. *Nature* **2008**, *452*, 301–310.
2. Fane, A. G.; Wang, R.; Hu, M. X. Synthetic Membranes for Water Purification: Status and Future. *Angew. Chem., Int. Ed.* **2015**, *54*, 3368–86.
3. Lee, K. P.; Arnot, T. C.; Mattia, D. A Review of Reverse Osmosis Membrane Materials for Desalination—Development to Date and Future Potential. *J. Membr. Sci.* **2011**, *370*, 1–22.
4. Peng, X.; Jin, J.; Nakamura, Y.; Ohno, T.; Ichinose, I. Ultrafast Permeation of Water through Protein-Based Membranes. *Nat. Nanotechnol.* **2009**, *4*, 353–357.
5. Fornasiero, F.; Park, H. G.; Holt, J. K.; Stadermann, M.; Grigoropoulos, C. P.; Noy, A.; Bakajin, O. From the Cover: Nanomaterials in Medicine Special Feature Sackler Colloquium: Ion Exclusion by Sub-2-nm Carbon Nanotube Pores. *Proc. Natl. Acad. Sci. U. S. A.* **2008**, *105*, 17250–17255.
6. Kalra, A. From the Cover: Osmotic Water Transport through Carbon Nanotube Membranes. *Proc. Natl. Acad. Sci. U. S. A.* **2003**, *100*, 10175–10180.
7. Chen, B.; Ma, Q.; Tan, C.; Lim, T.-T.; Huang, L.; Zhang, H. Carbon-Based Sorbents with Three-Dimensional Architectures for Water Remediation. *Small* **2015**, DOI: 10.1002/smll.201403729.
8. Zhou, M. J.; Nemade, P. R.; Lu, X. Y.; Zeng, X. H.; Hatakeyama, E. S.; Noble, R. D.; Gin, D. L. New Type of Membrane Material for Water Desalination Based on a Cross-Linked Bicontinuous Cubic Lyotropic Liquid Crystal Assembly. *J. Am. Chem. Soc.* **2007**, *129*, 9574–9575.
9. Rajesh, S.; Yan, Y.; Chang, H.-C.; Gao, H.; Phillip, W. A. Mixed Mosaic Membranes Prepared by Layer-by-Layer Assembly for Ionic Separations. *ACS Nano* **2014**, *8*, 12338–12345.
10. Agre, P. Aquaporin Water Channels. *Angew. Chem., Int. Ed.* **2004**, *43*, 4278–4290.
11. van Rijn, P.; Tutus, M.; Kathrein, C.; Mougin, N. C.; Park, H.; Hein, C.; Schürings, M. P.; Böker, A. Ultra-Thin Self-Assembled Protein-Polymer Membranes: A New Pore Forming Strategy. *Adv. Funct. Mater.* **2014**, *24*, 6762–6770.
12. Lu, Y.; Suzuki, T.; Zhang, W.; Moore, J. S.; Marin, B. J. Nanofiltration Membranes Based on Rigid Star Amphiphiles. *Chem. Mater.* **2007**, *19*, 3194–3204.

13. Yassin, M. A.; Appelhans, D.; Wiedemuth, R.; Formanek, P.; Boye, S.; Lederer, A.; Temme, A.; Voit, B. Overcoming Concealment Effects of Targeting Moieties in the Peg Corona: Controlled Permeable Polymersomes Decorated with Folate-Antennae for Selective Targeting of Tumor Cells. *Small* **2015**, *11*, 1580–1591.
14. Wen, L.; Jiang, L. Construction of Biomimetic Smart Nanochannels for Confined Water. *Natl. Sci. Rev.* **2014**, *1*, 144–156.
15. Tagliazucchi, M.; Azzaroni, O.; Igal, S. Responsive Polymers End-Tethered in Solid-State Nanochannels: When Nanoconfinement Really Matters. *J. Am. Chem. Soc.* **2010**, *132*, 12404–12411.
16. Pendergast, M. M. H.; Eric, M. V. A Review of Water Treatment Membrane Nanotechnologies. *Energy Environ. Sci.* **2011**, *4*, 1946–1971.
17. Hinds, B. J. Aligned Multiwalled Carbon Nanotube Membranes. *Science* **2004**, *303*, 62–65.
18. He, Z.; Zhou, J.; Lu, X.; Corry, B. Bioinspired Graphene Nanopores with Voltage-Tunable Ion Selectivity for Na^{+} and K^{+}. *ACS Nano* **2013**, *7*, 10148–10157.
19. Yoon, D.; Lee, C.; Yun, J.; Jeon, W.; Cha, B. J.; Baik, S. Enhanced Condensation, Agglomeration, and Rejection of Water Vapor by Superhydrophobic Aligned Multiwalled Carbon Nanotube Membranes. *ACS Nano* **2012**, *6*, 5980–5987.
20. Chen, Q.; Kong, X.; Li, J.; Lu, D.; Liu, Z. Electrokinetic Desalination Using Honeycomb Carbon Nanotubes (HC-CNTs): A Conceptual Study by Molecular Simulation. *Phys. Chem. Chem. Phys.* **2014**, *16*, 18941–18948.
21. Joshi, R. K.; Carbone, P.; Wang, F. C.; Kravets, V. G.; Su, Y.; Grigorieva, I. V.; Wu, H. A.; Geim, A. K.; Nair, R. R. Precise and Ultrafast Molecular Sieving through Graphene Oxide Membranes. *Science* **2014**, *343*, 752–754.
22. Sun, P.; Zheng, F.; Zhu, M.; Song, Z.; Wang, K.; Zhong, M.; Wu, D.; Little, R. B.; Xu, Z.; Zhu, H. Selective Trans-Membrane Transport of Alkali and Alkaline Earth Cations through Graphene Oxide Membranes Based on Cation-Pi Interactions. *ACS Nano* **2014**, *8*, 850–859.
23. Huang, J.-Q.; Zhuang, T.-Z.; Zhang, Q.; Peng, H.-J.; Chen, C.-M.; Wei, F. Permselective Graphene Oxide Membrane for Highly Stable and Anti-Self-Discharge Lithium−Sulfur Batteries. *ACS Nano* **2015**, *9*, 3002–3011.
24. Das, R.; Ali, M. E.; Abd Hamid, S. B.; Ramakrishna, S.; Chowdhury, Z. Z. Carbon Nanotube Membranes for Water Purification: A Bright Future in Water Desalination. *Desalination* **2014**, *336*, 97–109.
25. Das, R.; Hamid, S. B. A.; Ali, M. E.; Ismail, A. F.; Annuar, M. S. M.; Ramakrishna, S. Multifunctional Carbon Nanotubes in Water Treatment: The Present, Past and Future. *Desalination* **2014**, *354*, 160–179.
26. Mattia, D.; Leese, H.; Lee, K. P. Carbon Nanotube Membranes: From Flow Enhancement to Permeability. *J. Membr. Sci.* **2015**, *475*, 266–272.
27. Lee, H. D.; Kim, H. W.; Cho, Y. H.; Park, H. B. Experimental Evidence of Rapid Water Transport through Carbon Nanotubes Embedded in Polymeric Desalination Membranes. *Small* **2014**, *10*, 2653–2660.
28. Schoch, R. B. Transport Phenomena in Nanofluidic. *Rev. Mod. Phys.* **2008**, *80*, 839–883.
29. Sparreboom, W.; Berg, a. V. d.; Eijkel, J. C. T. Principles and Applications of Nanofluidic Transport. *Nat. Nanotechnol.* **2009**, *4*, 332–335.
30. Chan, W. F.; Chen, H. Y.; Surapathi, A.; Taylor, M. G.; Shao, X. H.; Marand, E.; Johnson, J. K. Zwitterion Functionalized Carbon Nanotube/Polyamide Nanocomposite Membranes for Water Desalination. *ACS Nano* **2013**, *7*, 5308–5319.
31. Tu, C. H.; Fang, Y. Y.; Zhu, J.; Van der Bruggen, B.; Wang, X. L. Free Energies of the Ion Equilibrium Partition of KCl into Nanofiltration Membranes Based on Transmembrane Electrical Potential and Rejection. *Langmuir* **2011**, *27*, 10274–10281.
32. Yang, H. Y.; Han, Z. J.; Yu, S. F.; Pey, K. L.; Ostrikov, K.; Karnik, R. Carbon Nanotube Membranes with Ultrahigh Specific Adsorption Capacity for Water Desalination and Purification. *Nat. Commun.* **2013**, *4*, 2220.
33. Duke, M. C.; O'Brien-Abraham, J.; Milne, N.; Zhu, B.; Lin, J. Y. S.; Diniz da Costa, J. C. Seawater Desalination Performance of Mfi Type Membranes Made by Secondary Growth. *Sep. Purif. Technol.* **2009**, *68*, 343–350.
34. Li, Q.; Bi, Q. y.; Lin, H. H.; Bian, L. X.; Wang, X. L. A Novel Ultrafiltration (UF) Membrane with Controllable Selectivity for Protein Separation. *J. Membr. Sci.* **2013**, *427*, 155–167.
35. Holmlin, R. E.; Chen, X. X.; Chapman, R. G.; Takayama, S. C.; Whitesides, G. M. Zwitterionic Sams That Resist Nonspecific Adsorption of Protein from Aqueous Buffer. *Langmuir* **2001**, *17*, 2841–2850.
36. Ramon, G. Z.; Wong, M. C. Y.; Hoek, E. M. V. Transport through Composite Membrane, Part 1: Is There an Optimal Support Membrane? *J. Membr. Sci.* **2012**, *415−416*, 298–305.
37. Pendergast, M. T. M.; Nygaard, J. M.; Ghosh, A. K.; Hoek, E. M. V. Using Nanocomposite Materials Technology to Understand and Control Reverse Osmosis Membrane Compaction. *Desalination* **2010**, *261*, 255–263.
38. Lau, W. J.; Ismail, A. F.; Misdan, N.; Kassim, M. A. A Recent Progress in Thin Film Composite Membrane: A Review. *Desalination* **2012**, *287*, 190–199.
39. Corry, B. Designing Carbon Nanotube Membranes for Efficient Water Desalination. *J. Phys. Chem. B* **2008**, *112*, 1427.
40. An, Q. F.; Sun, W. D.; Zhao, Q.; Ji, Y. L.; Gao, C. J. Study on a Novel Nanofiltration Membrane Prepared by Interfacial Polymerization with Zwitterionic Amine Monomers. *J. Membr. Sci.* **2013**, *431*, 171–179.
41. An, Q. F.; Ji, Y. L.; Hung, W. S.; Lee, K. R.; Gao, C. J. Amoc Positron Annihilation Study of Zwitterionic Nanofiltration Membranes: Correlation between Fine Structure and Ultrahigh Permeability. *Macromolecules* **2013**, *46*, 2228–2234.
42. Zhang, Q.; Huang, J. Q.; Qian, W. Z.; Zhang, Y. Y.; Wei, F. The Road for Nanomaterials Industry: A Review of Carbon Nanotube Production, Post-Treatment, and Bulk Applications for Composites and Energy Storage. *Small* **2013**, *9*, 1237–1265.
43. Zhang, Q.; Zhao, M. Q.; Huang, J. Q.; Liu, Y.; Wang, Y.; Qian, W. Z.; Wei, F. Vertically Aligned Carbon Nanotube Arrays Grown on a Lamellar Catalyst by Fluidized Bed Catalytic Chemical Vapor Deposition. *Carbon* **2009**, *47*, 2600–2610.
44. Qian, W. Z.; Wei, F.; Wang, Z. W.; Liu, T.; Yu, H.; Luo, G. H.; Xiang, L.; Deng, X. Y. Production of Carbon Nanotubes in a Packed Bed and a Fluidized Bed. *AIChE J.* **2003**, *49*, 619–625.
45. Liu, T. Y.; Zhang, R. X.; Li, Q.; Van der Bruggen, B.; Wang, X. L. Fabrication of a Novel Dual-Layer (PES/PVDF) Hollow Fiber Ultrafiltration Membrane for Wastewater Treatment. *J. Membr. Sci.* **2014**, *472*, 119–132.
46. Liu, T. Y.; Bian, L. X.; Yuan, H. G.; Pang, B.; Lin, Y. K.; Tong, Y.; Van der Bruggen, B.; Wang, X. L. Fabrication of a High-Flux Thin Film Composite Hollow Fiber Nanofiltration Membrane for Wastewater Treatment. *J. Membr. Sci.* **2015**, *478*, 25–36.
47. Van Der Bruggen, B.; Schaep, J.; Wilms, D.; Vandecasteele, C. A Comparison of Models to Describe the Maximal Retention of Organic Molecules in Nanofiltration. *Sep. Sci. Technol.* **2000**, *35*, 169–182.